



**HAL**  
open science

## Slip and cornering stiffnesses observation for the stability assessment of off-road vehicles

D. Denis, A. Nizard, B. Thuilot, R. Lenain

► **To cite this version:**

D. Denis, A. Nizard, B. Thuilot, R. Lenain. Slip and cornering stiffnesses observation for the stability assessment of off-road vehicles. International Conference on Mediterranean Green Energy Forum, Mar 2015, Marrakech, Morocco. hal-01368574

**HAL Id: hal-01368574**

**<https://hal.science/hal-01368574>**

Submitted on 19 Sep 2016

**HAL** is a multi-disciplinary open access archive for the deposit and dissemination of scientific research documents, whether they are published or not. The documents may come from teaching and research institutions in France or abroad, or from public or private research centers.

L'archive ouverte pluridisciplinaire **HAL**, est destinée au dépôt et à la diffusion de documents scientifiques de niveau recherche, publiés ou non, émanant des établissements d'enseignement et de recherche français ou étrangers, des laboratoires publics ou privés.

# Slip and Cornering Stiffnesses Observation for the Stability Assessment of Off-road Vehicles

Dieumet Denis<sup>2,3</sup>, Ange Nizard<sup>2,3</sup>, Benoit Thuilot<sup>2,3</sup> and Roland Lenain<sup>1</sup>

**Abstract**—A real-time observer allowing to check the stiffnesses in the longitudinal and lateral directions of the contact between natural soils and tires is presented. This work responds to the need of active security devices for off-road vehicles that are subject to instability, leading sliding and rollover. The algorithm has been experimented on a grape harvester in real conditions. The results of this low-cost observer are compared to precise measures acquired with expensive sensors and validate that the driver can be informed when the situation becomes dangerous.

## I. INTRODUCTION

Statistical studies show that vehicle instability is one of the main sources of serious accidents in agricultural works [1]. In this paper, considered causes of instability are related to the terrain, the vehicle and the driver. Firstly, agricultural exploitation of very hilly terrain has become usual and drivers are regularly forced to push the machines to their stability limits. The risk of stability loss is even higher if the soil has poor traction capabilities. Secondly, a machine can be originally not very stable due to its disproportionate geometry required by the specific agricultural work it has to achieve, like grape harvesters which have a high and variable center of gravity. Finally, the instability is occasionally produced by the driver himself by poor driving skills or inappropriate reactions to unexpected situations, etc.

Getting into a spin and making a rollover is the main outcome of both lateral and longitudinal instabilities. Indeed, the longitudinal instability itself is often followed by a lateral one because of the speed increase. In order to improve the safety of these machines, passive devices have been developed. One can mention heavy structures (e.g. rollover protection structures [1]) creating an incompressible safe zone around the driver, but they are too restrictive in most cases. For instance, such structures increase instability of small vehicles and need to be excessively strong on heavy machines. Furthermore, they are ineffective if the driver does not use the seat-belt.

Driving assistance systems (such as ESP or ABS) [5] have been deeply studied for on-road vehicles and successfully improve safety. These systems usually assume that the vehicle Center of Gravity (CG) height is low and that the vehicles are operating on smooth and level terrain. Since

these assumptions are not satisfied when considering off-road vehicles with a high CG, such devices cannot be applied directly.

Consequently, this paper presents an observer dedicated to off-road vehicles to assess the risk of hurtling down in the longitudinal direction and of lateral skidding. In order to investigate their longitudinal and lateral stability and eventually develop an active security device. In previous work [4], a proactive device has been developed to estimate the rollover risk before any attempt of the driver to steer the vehicle and then discouraging him to steer too much with a force feedback in the steering wheel. In order to supplement this device, it could also be interesting to know the most effective slip ratio dynamically to adapt ABS and ESP systems to off-road vehicles. Here, the chosen criteria to assess the lateral and longitudinal stability are the cornering and the slip stiffnesses, computed at each tire with an algorithm based on inexpensive sensors and a linearized tire model. To achieve this, it is necessary to determine the longitudinal slip ratio at each tire, the global sideslip angle and the forces in lateral, longitudinal (traction) and vertical (load) directions.

First, we present our modeling choices regarding the vehicle and the contact between the ground and the tires. Then, a detailed description of the observer is exposed, followed by a selection of illustrative experiments.

## II. SYSTEM MODELING

It appears that the use of a complete 3D dynamic model may be hardly tractable and time consuming from an observation point of view [12] and with a low cost perception system. As a result, this paper proposes to describe the vehicle motion from partial dynamic multiscale models and linear contact models. Thanks to this approach, lateral and longitudinal dynamics of the vehicle can be decoupled, as illustrated below.

### A. Lateral Vehicle Dynamic Model

The lateral vehicle dynamic is modeled in the yaw frame as depicted in Fig. 1. In this frame, the vehicle is considered as a bicycle (each axle is viewed as a sole wheel) and its motion is described perpendicularly to a plane defined by the wheel/ground contact points. The influence of the vehicle inclination is accounted by incorporating the lateral component of the gravity force  $P_y = mg \sin \alpha_r$ , where  $\alpha_r$  is the lateral bank angle of the terrain,  $g$  is the gravitational constant and  $m$  is the vehicle mass.

<sup>1</sup>Irstea, 24 avenue des Landais, 63170 Aubière, France

<sup>2</sup>CNRS, UMR 6602, Institut Pascal, 63171 Aubière, France

<sup>3</sup>Clermont Université, Université Blaise Pascal, Institut Pascal, BP 10448, 63000 Clermont-Ferrand, France

dieumet.denis@univ-bpclermont.fr, ange.nizard@gmail.com,  
benoit.thuilot@univ-bpclermont.fr, roland.lenain@irstea.fr

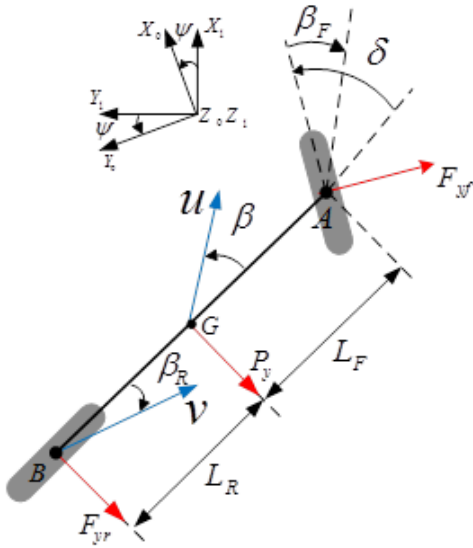


Fig. 1. Single-track vehicle model

In order to avoid the use of complex tire/soil interaction models such as Pacejka [9] or LuGre [10], lateral contact forces at each wheel  $F_{yf}$  and  $F_{yr}$  are assumed to be in linear relation with corresponding sideslip angles  $\beta_F$  and  $\beta_R$  and this leads to equation (1)

$$\begin{cases} F_{yf} = C_f \beta_F \\ F_{yr} = C_r \beta_R \end{cases} \quad (1)$$

with  $C_f, C_r > 0$ , the cornering stiffnesses for respectively the front and the rear axles. The main advantage of this linear model is its reduced number of parameters to be estimated.

Assuming that sideslip angles remain small (i.e  $\cos \beta \simeq 1$  and  $\sin \beta \simeq \beta$ ) yields to the equation (2), where  $L_F$  and  $L_R$  are respectively the front and rear vehicle half-wheelbases,  $\beta$  is the global sideslip angle,  $\dot{\psi}$  is the yaw rate,  $u$  is the linear velocity at the center of gravity  $G$  and  $\delta$  is the steering angle.

$$\begin{cases} \beta_R = \beta - \frac{L_R \dot{\psi}}{u} \\ \beta_F = \beta + \frac{L_F \dot{\psi}}{u} - \delta \end{cases} \quad (2)$$

Then, by neglecting the contribution of the longitudinal forces to the yaw motion and considering the linear tire contact model (1), the application of the Fundamental Principle of Dynamics to the bicycle model sketched in Fig. 1 yields vehicle motion equations (3) in the yaw frame.

$$\begin{cases} \dot{\beta} = \frac{-C_f \beta_F - C_r \beta_R - m g \sin \alpha_r}{u m} - \dot{\psi} \\ \ddot{\psi} = \frac{L_R C_r \beta_R - L_F C_f \beta_F \cos \delta}{I_z \cos \alpha_r} \end{cases} \quad (3)$$

Finally, the equation (3) can be written as the state equa-

tion (4)

$$\begin{cases} \dot{X}(t) = A X(t) + B U(t) \\ Y(t) = C X(t) + D U(t) \end{cases} \quad (4)$$

with:  $X = [\dot{\psi} \ \beta]^T$ ,  $U = [\delta \ \sin \alpha_r]^T$ ,

$$A(C_f, C_r) = \begin{bmatrix} \frac{-C_f L_F^2 + C_r L_R^2}{u I_z} & \frac{C_r L_R - C_f L_F}{I_z} \\ \frac{C_r L_R - C_f L_F}{u^2 m} - 1 & -\frac{C_f + C_r}{u m} \end{bmatrix}$$

$$B(C_f, C_r) = \begin{bmatrix} \frac{L_F C_f}{I_z} & 0 \\ \frac{C_f}{u m} & -\frac{g}{u} \end{bmatrix}, \quad C = [1 \ 0] \text{ and } D = [0]$$

### B. Longitudinal Vehicle Dynamic Model

Above, a classical bicycle model was used to evaluate the lateral dynamic of the vehicle. But, the linear and rotational speed of each wheel may be very different, as well as their slip ratios and stiffnesses, prohibiting in any way to aptly estimate overall values. This is why the two-track model shown in Fig. 2 is chosen for evaluating the longitudinal vehicle dynamic. Similarly to the lateral dynamics, the longitudinal terrain slope  $\alpha_p$  is considered by incorporating the longitudinal component of the gravity force  $P_x = m g \sin \alpha_p$  and the contribution of lateral forces to the longitudinal motion is neglected.

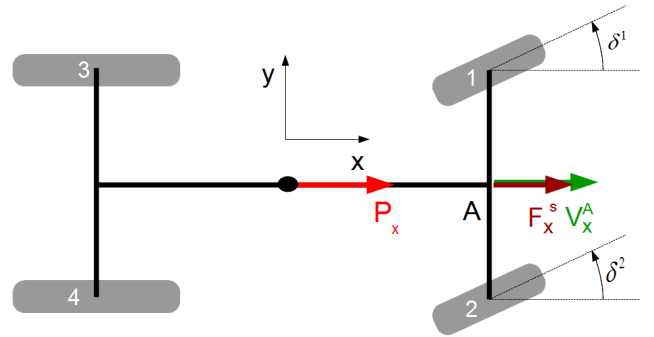


Fig. 2. Two-track vehicle model

The longitudinal slip ratio  $g_x$  of each wheel is given by the equation (5) defined by the Society of Automotive Engineer (SAE) [11].

$$g_x = \frac{r_e \omega - V_w}{\max(|r_e \omega|, |V_w|)} \quad (5)$$

with  $V_w$  the linear speed at the wheel center,  $\omega$  its rotational speed and  $r_e$  its effective radius. Then, the longitudinal force  $F_x$  generated at each wheel is inferred from the equation (6)

$$F_x = C_x g_x \quad (6)$$

where  $C_x > 0$  is the slip stiffness.

As it can be seen, a linear contact model (6) is herein chosen as it was the case for the evaluation of lateral

dynamics previously (see equation (1)). These pneumatic-soil interaction models are very simple, but the on-line estimation of  $C_i$ , with  $i = \{x, f, r\}$ , allows to account for ground contact variations and non-linearities at the same time without numerous and expensive sensors. As an example, the Fig. 3 presents two different  $C_x$  values for a same tire/ground pair subject to two slip ratios; blue dots represent the corresponding operating points. Afterwards,  $C_x$  is the criterion assessing the longitudinal grip conditions, i.e. the risk of control loss.

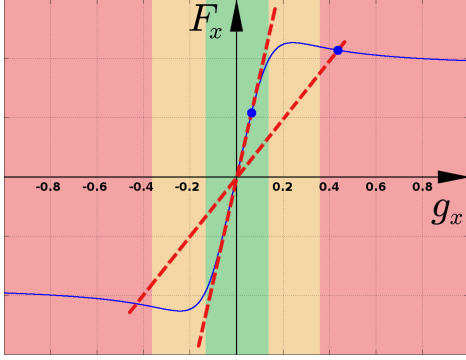


Fig. 3. Considered linear longitudinal tire model (6) in red compared to a Pacejka model in blue. Background colors highlight the three major operating areas: pseudo-slip in green to saturation in pink

Finally, regardless of the rolling resistance and the forces that the ground deformation opposes to the tires (introducing, in the worst case, a bias that makes the algorithm to be presented pessimistic about the stability), the longitudinal dynamic is governed by (7).

$$\dot{V}_x = \frac{F_x^s}{m} + g \sin(\alpha_p) \quad (7)$$

where  $\dot{V}_x$  is the longitudinal acceleration of the vehicle and  $F_x^s$  is the sum of the longitudinal tire forces.

### III. LONGITUDINAL STIFFNESS OBSERVATION

The algorithm presented in this section for estimating the slip stiffness is composed of several estimators and observers graphically summarized in Fig. 4.

Based on the vehicle longitudinal dynamic equation (7), the observer computes the overall longitudinal traction force  $F_x^s$  generated by the wheels. It is then distributed to obtain each  $F_x$  according to the mass distribution on the four wheels through two load transfer coefficients ( $LLT_x$  and  $LLT_y$  which are computed thanks to the algorithm developed in [8] and the longitudinal ground slope  $\alpha_p$  calculated with the method used in [4]). In parallel, basic kinematic relations derived from the rigid vehicle model allow to estimate each  $V_w$  and then the four longitudinal slip ratios  $g_x$ . Finally, the observer uses these outputs to determine the four longitudinal stiffnesses  $C_x$ . Since the state of each wheel is not representative of the overall vehicle stability, the four stiffnesses are combined to get a meaningful criterion.

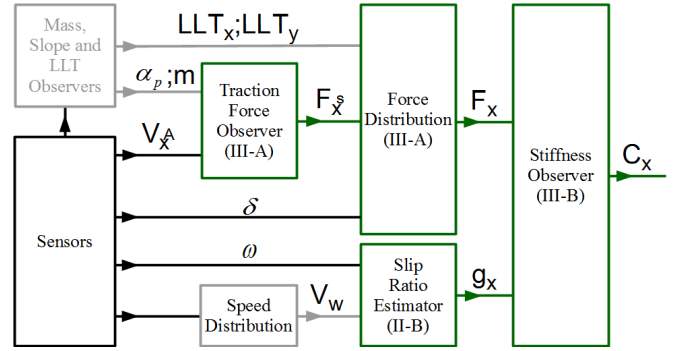


Fig. 4. Overview of the observers. Black boxes and links are for measured values; gray parts are for values observed by previously developed algorithms and green ones for those currently presented

#### A. Longitudinal forces observation

The ultimate goal is to observe the contact stiffness at each tire through the relation (6). First, it is therefore necessary to estimate the traction force of each wheel in real-time. Since it is not possible to do so without costly and numerous sensors, we propose in the first place to observe the overall traction force created by the four tires via the longitudinal vehicle model (7).

Let  $\hat{V}_x$ ,  $\widehat{V}_x$  and  $\widehat{F}_x^s$  be the estimated values of  $\dot{V}_x$ ,  $V_x$  and  $F_x^s$  respectively. Forcing  $\widehat{V}_x = V_x - \widehat{V}_x$  to tend toward 0 according to  $\dot{\widehat{V}}_x = -k_f \widehat{V}_x$  with  $k_f > 0$  gives us the observer (8):

$$\begin{cases} \dot{\widehat{V}}_x &= \dot{V}_x + k_f (V_x - \widehat{V}_x) \\ \widehat{F}_x^s &= m (\dot{\widehat{V}}_x - g \sin(\alpha_p)) \end{cases} \quad (8)$$

This formulation ensures a more robust estimation of  $F_x^s$  than a direct measurement with the IMU or deriving the speed measurement.

To reach per wheel force, we then make the assumption that  $F_x^s$  is distributed according to the vertical load distribution. The latter is computed thanks to the algorithm developed in [8] that gives the lateral load transfer coefficient named  $LLT_y$ . The longitudinal load transfer  $LLT_x$  is defined similarly to  $LLT_y$ , yielding (9):

$$\begin{aligned} LLT_y &= \frac{(F_z^2 + F_z^4) - (F_z^1 + F_z^3)}{F_z^s} \\ LLT_x &= \frac{(F_z^1 + F_z^2) - (F_z^3 + F_z^4)}{F_z^s} \end{aligned} \quad (9)$$

Each of them is comprised in the range [-1;1]. The final distribution (10) of the longitudinal forces is then:

$$\begin{cases} \widehat{F}_x^1 &= \widehat{F}_x^s \left( \frac{(1+LLT_x)(1-LLT_y)}{4 \cos(\delta^1)} \right) \\ \widehat{F}_x^2 &= \widehat{F}_x^s \left( \frac{(1+LLT_x)(1+LLT_y)}{4 \cos(\delta^2)} \right) \\ \widehat{F}_x^3 &= \widehat{F}_x^s \left( \frac{(1-LLT_x)(1-LLT_y)}{4} \right) \\ \widehat{F}_x^4 &= \widehat{F}_x^s \left( \frac{(1-LLT_x)(1+LLT_y)}{4} \right) \end{cases} \quad (10)$$

The estimations for the two front wheels need to be corrected because of the steering angles; it is done in (10) by applying the coefficient  $\frac{1}{\cos(\delta^i)}$ .

### B. Longitudinal stiffness observation

Since slip ratios and traction forces have been estimated at each wheel, (6) can be used to compute the four longitudinal stiffnesses. Let  $\widehat{C}_x$  be the current estimation of  $C_x$ . Then,  $\widehat{C}_x g_x$  is a ‘‘prediction’’ of the longitudinal force. The error between the predicted value  $\widehat{C}_x g_x$  and  $\widehat{F}_x$  considered as a sensed value is called  $\widetilde{F}_x$ ; it can be written as (11):

$$\widetilde{F}_x = \widehat{C}_x g_x - \widehat{F}_x \quad (11)$$

According to the MIT rule (see [6]), the adaptation law of  $\widehat{C}_x$  that makes  $\widetilde{F}_x$  tend toward 0 is (12):

$$\dot{\widehat{C}}_x = -k_c \frac{\partial \widetilde{F}_x}{\partial \widehat{C}_x} \widetilde{F}_x \quad (12)$$

where  $k_c > 0$ . Injecting (11) into (12) yields to (13):

$$\dot{\widehat{C}}_x = -k_c g_x (\widehat{C}_x g_x - \widehat{F}_x) \quad (13)$$

The convergence of  $\widehat{C}_x$  is ensured if  $C_x$  is slowly varying. This observer has the advantage to be never singular, even if  $g_x$  tends toward 0 which may occur when the vehicle stops. In that case, the stiffness update is frozen in a natural way until the vehicle restarts. It can be noted that the initialization of  $\widehat{C}_x$  is not critical thanks to the fast convergence of the observer (tuned by  $k_c$ ).

## IV. LATERAL GRIP CONDITIONS OBSERVATION

In this section, a backstepping observer is developed in order to evaluate the risk of lateral skidding. Sketched in Fig. 5, it is based both on a yaw model and a linear contact forces model. Thanks to this observer, the cornering stiffnesses, representative of lateral grip conditions and difficult to measure directly in off-road environments, are estimated in real-time. Ultimately, the observed cornering stiffness is used as a relevant criterion to warn against the vehicle skidding risk.

### A. Observability proof

Before any development of an observer, it is necessary to verify if the system is observable, i.e., if from measured data, the state variables can be reconstructed.

These measured data are the yaw rate, the vehicle velocity and the steering angle. The lateral terrain inclination  $\alpha_r$  is computed with the method described in [4]. These only four variables do not permit to estimate  $C_f$  and  $C_r$  separately. Thus, for observability reasons, they are supposed to be equal to a global virtual cornering stiffness  $C_e$ , i.e.,  $C_f = C_r = C_e$ .

The Kalman observability matrix  $\mathcal{O}_{obs}$  for the state space model (4) is:

$$\mathcal{O}_{obs} = \begin{bmatrix} C \\ CA \end{bmatrix} = \begin{bmatrix} 1 & 0 \\ -\frac{(L_R^2 + L_F^2)C_e}{uI_z} & \frac{(L_R - L_F)C_e}{I_z} \end{bmatrix} \quad (14)$$

It can be checked that  $\mathcal{O}_{obs}$  is a full rank matrix provided that:

- the inclination of the ground is less than  $90^\circ$ ,
- the vehicle speed  $u$  is non-zero,
- and the term  $(L_R - L_F)$  is non-zero, because  $C_e$  is strictly positive by definition.

It can be noticed that these three conditions are simultaneously true in the context of our study. Evidently, the terrain slope is always well below  $90^\circ$  and the observation is frozen at zero speed because the vehicle is stable when it is stopped. Finally, the center of gravity is always located a little further forward on commercial tractors [13]. Therefore, the front half-wheelbase  $L_F$  of the vehicle is shorter than the rear one  $L_R$ . As a result, it can be concluded that the term  $(L_R - L_F)$  is always non-zero.

The observability of the state space model (4) is then proved. Consequently, the cornering stiffness can be observed in the next section.

### B. Cornering stiffness observation

As sketched in Fig. 5, the observer is developed on a backstepping approach divided into three steps.

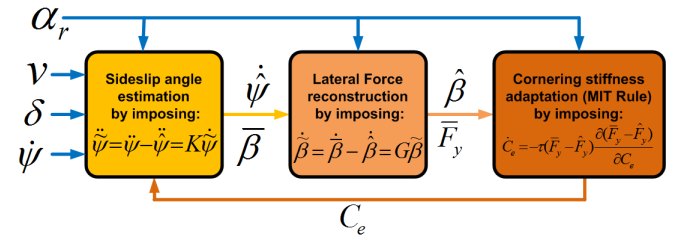


Fig. 5. Lateral Dynamic Observer overview

#### a) Global sideslip angle estimation

The first part consists in computing a virtual measurement of the global sideslip angle (denoted  $\bar{\beta}$  in Fig. 5). More precisely,  $\bar{\beta}$  is derived by imposing the convergence of the estimated yaw rate  $\hat{\psi}$  to the measured one  $\dot{\psi}$  according to the following exponential dynamic:

$$\ddot{\psi} = \ddot{\psi} - \dot{\psi} = K\dot{\psi}, \quad K < 0 \quad (15)$$

where  $\ddot{\psi}$  is derived from the measured yaw rate. Injecting (15) into the second equation in (3) leads to the following expression for  $\bar{\beta}$ :

$$\bar{\beta} = \frac{\ddot{\psi} - K\dot{\psi} - a_{11}(C_e)\dot{\psi} - b_1(C_e)\delta}{a_{12}(C_e)} \quad (16)$$

Since  $\bar{\beta}$  ensures that  $\hat{\psi}$  converges to the actual value  $\dot{\psi}$  supplied by the inertial measurement unit, it can then be considered as a relevant estimation of the actual

global sideslip angle.

### b) Global Lateral Force Reconstruction

In the second step, the overall lateral contact force:

$$F_y = C_e(\beta_F + \beta_R) \quad (17)$$

is treated as a control variable. A control law, denoted  $\overline{F}_y$  in Fig. 5, is then designed in order to impose the convergence of the estimated global sideslip angle  $\hat{\beta}$  to the virtual measure  $\tilde{\beta}$  according to the following exponential dynamic:

$$\dot{\tilde{\beta}} = \dot{\hat{\beta}} - \dot{\beta} = G\tilde{\beta}, \quad G < 0 \quad (18)$$

Injecting (18) in the first equation (3) leads to:

$$\overline{F}_y = -um(\dot{\psi} + \frac{g}{u} \sin \alpha_r + \dot{\tilde{\beta}} - G\tilde{\beta}) \quad (19)$$

where  $\dot{\tilde{\beta}}$  is the numerical derivative of  $\tilde{\beta}$ .

Since  $\overline{F}_y$  ensures that  $\hat{\beta}$  converges to the virtual measurement  $\tilde{\beta}$ , it can be regarded as a relevant estimation of the overall lateral contact force.

### c) Cornering stiffness adaptation

Finally, since the cornering stiffness  $C_e$  can be considered as a slow varying parameter, it can be obtained by imposing the convergence of an estimated force  $\widehat{F}_y$ , designed from (17),

$$\widehat{F}_y = \widehat{C}_e(\widehat{\beta}_F + \widehat{\beta}_R) \quad (20)$$

to the virtual measurement  $\overline{F}_y$  according to the *MITRule* as presented in [6].

$$\begin{cases} \dot{\widehat{C}}_e &= -\tau(\overline{F}_y - \widehat{F}_y) \frac{\partial(\overline{F}_y - \widehat{F}_y)}{\partial \widehat{C}_e} \\ &= -\tau(\overline{F}_y - \widehat{F}_y)(\widehat{\beta}_F + \widehat{\beta}_R) \end{cases} \quad (21)$$

where  $\overline{F}_y$  is given by (19) and  $\tau$  is a strictly positive gain. The front and the rear sideslip angles  $\widehat{\beta}_F$  and  $\widehat{\beta}_R$  are inferred from the equation (2) by using the estimated value of the overall sideslip angle  $\hat{\beta}$ .

## V. EXPERIMENTAL RESULTS

### A. Experimental test bed

The experimental vehicle used to validate the proposed algorithms for the lateral and longitudinal grip estimation is a grape harvester manufactured by Gregoire SAS, depicted in Fig. 6. This machine is able to climb slopes up to  $15^\circ$  and is equipped with an “active suspension” system for tilt correction – this latter is not dynamic, the correction is triggered occasionally by the driver. The mass may vary from 9 to 12 tons depending on harvest load. It is actuated by four hydraulic engines connected by the TwinLock™ system, enabling the optimization of the torque repartition.

A CAN bus is settled on the vehicle, providing access to the steering angle  $\delta$  and wheel velocities  $\omega$ . In addition, the



Fig. 6. Experimental vehicle equipped with low cost sensors used for observation: IMU (top right) and speed sensor (bottom right)

observer described in this paper requires the knowledge of the current linear velocity  $u$ , vehicle accelerations and yaw rate. They are measured by a Xsens MTi IMU and a Doppler radar (GMH Engineering DRS1000). This constitutes the “low cost” sensors used by the proposed approach. The algorithms are here implemented on a conventional laptop at a sampling frequency of 10Hz.

In order to analyze the capabilities of the proposed approach, two “expensive” dynamometers have been mounted on the two left wheels, providing the six components (forces and torques) at the wheel centers. These prototypes have been tested and calibrated on a dedicated test bed and the longitudinal and lateral components thus obtained are considered in the sequel as reference measured values of the longitudinal and lateral forces.

### B. Results related to the slip stiffness observer

#### 1) Test description:

The output of the observer proposed in this paper to estimate the longitudinal vehicle dynamic is investigated thanks to experiments carried out on a field with an average slope of 8 degrees (see right of the figure 7). An artificial “sliding area” has been created with a wet tarpaulin placed on the ground. It introduces an important decrease of grip conditions. In this experiment, the vehicle moves at a constant cruise speed, climbs the slope, operates a half turn and goes back in the slope – as depicted by the trajectory on the left of figure 7. In addition, two attempts to stop the vehicle have been achieved on the “sliding areas” (in both directions) leading to important sliding.

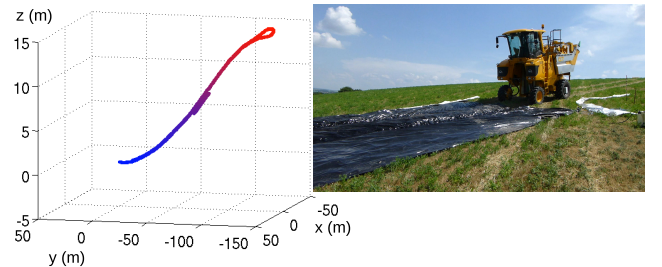


Fig. 7. Trajectory (left) and experimental field (right)

### 2) Global longitudinal force analysis:

The first step of the proposed approach aims at achieving an estimation of the overall longitudinal force  $F_x^s$  (issued from observer (8)) representative of the overall vehicle longitudinal behavior. The Fig. 8 shows the estimated longitudinal force in dashed red line during the three phases of the test: going straight up, half turn, and coming back down. It also shows in solid black line the measured data delivered by the dynamometers.

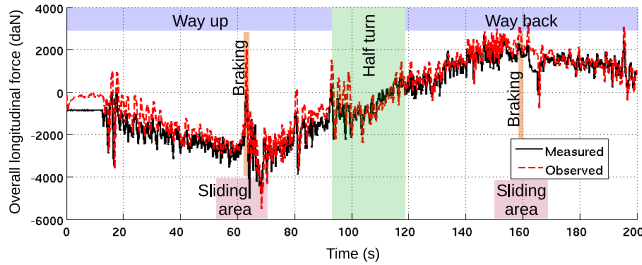


Fig. 8. Overall longitudinal force: estimated vs measured

As it can be seen, there is an accurate superposition of the observed and measured overall forces despite the conditions (slope and turns) and disturbances (braking and sliding areas). In particular, one can see that the observed force is able to relevantly describe the fast variations when crossing the sliding areas. It uses a simple set of sensors contrarily to the results obtained with the expensive dynamometers.

### 3) Longitudinal grip conditions adaptation analysis:

The estimation of the overall longitudinal force is a first step. This work indeed aims at estimating the grip conditions in order to prevent off-road vehicles and robots to lose control.

The Fig. 9 presents the average of the four adapted stiffnesses issued from the adaptation law (13). It can be noticed when the vehicle stops while crossing the sliding area, that the average adapted stiffness drastically decreases (around 65s and 160s) showing a lack of grip, which may be dangerous for the vehicle controllability. The adaptation process succeeds in sensing the modification of wheel/ground contact conditions. This adaptation is not only representative of the varying grip conditions, but also of the non-linear behavior of the tire: when a vehicle starts and stops, the sliding is indeed important and the tire is operating in its non-linear area (see Fig. 3). As a result, the stiffness decreases to account for the non-linearity. This is what happens around 65s, the vehicle stops while climbing the slope and restarts rapidly, making the wheel spinning and the stiffness falling to almost zero. In the half turn, the adaptation of the stiffness is stopped because of the very high steering angle that prevents the observer to work properly.

## C. Results related to the cornering stiffness observer

### 1) Trial description:

In order to investigate several aspects of the lateral stiffness observer, a typical test pointing out the lateral instability risk

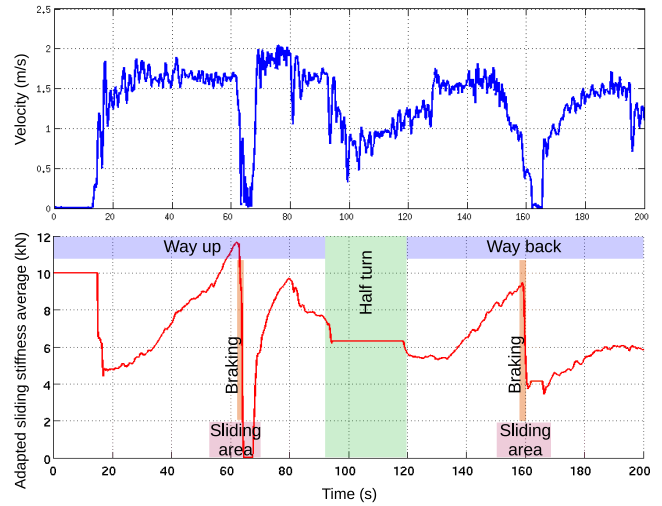


Fig. 9. Vehicle speed (top) and average of the four adapted longitudinal stiffnesses  $\bar{C}_x$  (bottom)

is realized with the previously described grape harvester. As depicted in Fig. 10, the machine moves on an irregular terrain with a slope part of  $10^\circ$  highlighted by the yellow strip on the trajectory. The attitude of the machine when moving on this sloping part is shown on the right of this figure. The trajectory has been achieved at a speed of  $1m/s$ . The inclination correction has been actuated during the straight lines (one time during going away and one time during the way back) in order for the vehicle structure to be as horizontal as possible. The elevation of the vehicle centre of gravity is of course impacted by these successive corrections.

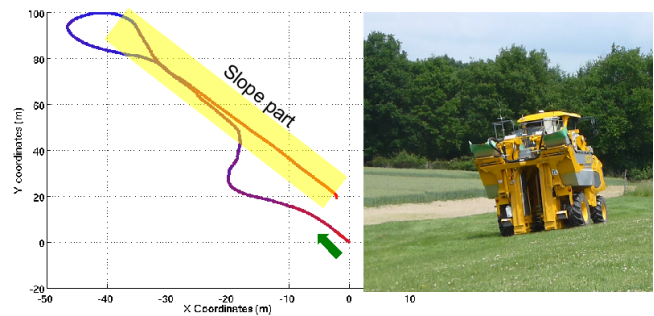


Fig. 10. Test background

### 2) Analysis of the estimation of the global lateral force:

The Fig. 11 compares the estimated global lateral force obtained from the observer (19) (red line) and the one measured with the dynamometric sensors (black line). Despite significant variations in the actual lateral force due to the slope, the inclination correction and the half-turn, an accurate overlap between estimated and measured efforts can be noticed, so that the estimated lateral force can be confidently used to estimate the cornering stiffness, even in harsh conditions.

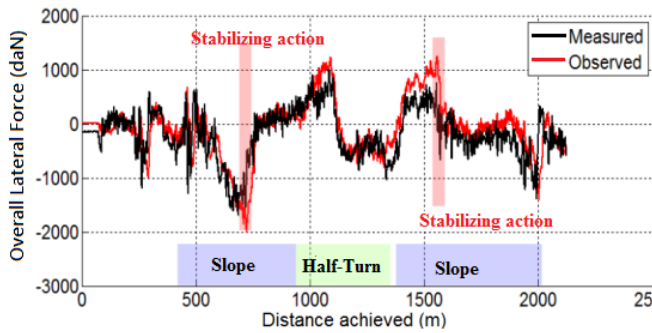


Fig. 11. Comparison of the estimated and measured overall lateral force

### 3) Analysis of the adaptation of lateral grip conditions:

The estimated cornering stiffness issued from the adaptation law (21) is reported in Fig. 12. It described the mobilized adherence, that is to say the adhesion currently used at the interface tire-soil: a low value means that the wheels are likely to slip sideways. The observed cornering stiffness may therefore be used as a relevant criterion to warn against a skidding risk.

It could be noticed that each inclination correction leads to a

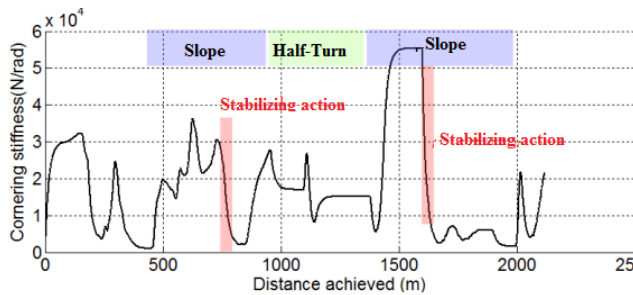


Fig. 12. Overall Cornering Stiffness

skidding risk, revealing its ambivalent influence with respect to the vehicle lateral stability. On one hand, the correction of the vehicle inclination reduces the risk of rollover, as it has been shown in previous work [8]. However, on the other hand, this correction decreases the mobilized adherence. Indeed, during the motion on the sloping terrain, the tires are subject to non-negligible lateral forces. Prior to the inclination correction (between 500 to 800 meters and 1400 to 1600 meters), a high level of adherence is observed. As soon as the attitude is corrected so that the vehicle structure returns horizontal (at abscissae 800 and 1600 meters), it can be noted that the adherence is greatly reduced. The attitude correction is therefore detrimental to adhesion.

## VI. CONCLUSION

This paper proposes observers dedicated to the estimation of the longitudinal and lateral grip conditions for off-road vehicles. It uses low cost sensors, making it easily implementable on vehicles and robots. Each observer is decomposed into several steps: for the estimation of the longitudinal grip conditions, the overall longitudinal force is then first observed using exteroceptive sensors; this overall force is

distributed on each wheel; next, with a measurement of the wheels slip ratios, an adaptation law computes the variations of the longitudinal grip conditions in real-time. Similarly for the lateral grip conditions, a backstepping observer is used to estimate successively the global sideslip angle, the overall lateral contact force and finally the cornering stiffness.

The performances of the proposed algorithms have been validated in full scale experiments and the forces estimation has been compared to measures supplied by expensive sensors – a ground truth. The results validate the capability of the algorithms to detect modifications of grip conditions caused by ground changes or by entering the non-linear operating area of the tires. These estimations permit to evaluate the dangerousness and the risk of a control loss, so that the driver can be warned (objective of the research project). Finally, these adaptive algorithms are intended to be used through active security devices in order to improve traction and braking control of off-road mobile robots.

## ACKNOWLEDGMENT

The work proposed in that paper is part of the project ActiSurTT funded by the French National Research Agency (ANR). It received the support of French Agricultural Social Insurance (CCMSA) and French Ministry of Agriculture.

## REFERENCES

- [1] J. M. DeGroot, C. Isaacs, W. Pickett, et al. Patterns of fatal machine rollovers in Canadian agriculture, *Journal of Agricultural Safety and Health*, 2011, vol. 31, no 3, pp. 97–102.
- [2] F. Gustafsson, Slip-based tire-road friction estimation, *Automatica*, 1997, vol. 33, no 6, pp. 1087–1099.
- [3] C. R. Carlson and J. C. Gerdes, Consistent nonlinear estimation of longitudinal tire stiffness and effective radius, *IEEE Transactions on Control Systems Technology*, 2005, vol. 13, no 6, pp. 1010–1020.
- [4] M. Richier, R. Lenain, B. Thuilot and C. Debain, On-line estimation of a stability metric including grip conditions and slope: Application to rollover prevention for All-Terrain Vehicles, *IEEE/RSJ International Conference on Intelligent Robots and Systems (IROS)*, 2011, pp. 4569–4574.
- [5] R. Bosch, *Driving Stability Systems: Bosch Technical Instruction*, Robert Bosch GmbH, 2005.
- [6] K. J. Astrom and B. Wittenmark, *Adaptive Control*, 2nd edition, Addison-Wesley Longman Publishing Co., Inc., Boston, USA, 1994.
- [7] K. Huh, S. Lim, J. Jung, D. Hong et al. Vehicle Mass Estimator for Adaptive Roll Stability Control, *SAE Technical Paper 2007-01-0820*, 2007.
- [8] D. Denis, B. Thuilot, R. Lenain, et al. Preserving stability of huge agriculture machines with internal mobilities: Application to a grape harvester, *International Conference on Agricultural Engineering*, Valencia, Spain, 2012.
- [9] H. B. Pacejka, *Tire and vehicle dynamics*, Society of Automotive Engineers, 2002.
- [10] C. Canudas de Wit and P. Tsiotras, Dynamic tire friction models for vehicle traction control, *IEEE Conference on Decision and Control*, 1999, vol. 4, pp. 3746–3751.
- [11] C. R. Carlson and J. C. Gerdes, Nonlinear estimation of longitudinal tire slip under several driving conditions, *In Proc. of the American Control Conference (ACC)*, Denver, USA, 2003
- [12] G. Genta, *Motor Vehicle Dynamics: Modeling and Simulation*, World Scientific, 1997
- [13] J. M. Stellman, *Encyclopaedia of Occupational Health and Safety*, International Labour Office, Geneva, Switzerland, 1998